Available online at www.sciencedirect.com

ScienceDirect

Geochimica et Cosmochimica Acta 149 (2015) 103–114

Geochimica et Cosmochimica Acta

www.elsevier.com/locate/gca

Net subterranean estuarine export fluxes of dissolved inorganic C, N, P, Si, and total alkalinity into the Jiulong River estuary, China

Guizhi Wang [a,b,*], Zhangyong Wang [c], Weidong Zhai [a,d], Willard S. Moore [e], Qing Li [a], Xiuli Yan [b], Di Qi [c], Yuwu Jiang [a]

[a] State Key Laboratory of Marine Environmental Science, Xiamen University, Xiamen, China
[b] College of Ocean and Earth Sciences, Xiamen University, Xiamen, China
[c] College of the Environment and Ecology, Xiamen University, Xiamen, China
[d] National Marine Environmental Monitoring Center, Dalian, China
[e] Department of Earth and Ocean Sciences, University of South Carolina, Columbia, SC, USA

Received 21 February 2014; accepted in revised form 1 November 2014; Available online 8 November 2014

Abstract

To evaluate geochemical impacts of the subterranean estuary (STE) on the Jiulong River estuary, China, we estimated seasonal fluxes of subterranean water discharge into the estuary based on the mass balance of radium isotopes and net subterranean export fluxes of dissolved inorganic C (DIC), N (DIN), Si (DSi), soluble reactive phosphorus (SRP), and total alkalinity (TA). Based on ^{226}Ra data, the subterranean discharge (in 10^7 m^3 d^{-1}) was estimated to be 0.29–0.60 in the spring, 0.69–1.44 in the summer, 0.45–0.93 in the fall, and 0.26–0.54 in the winter. This was equivalent to 8–19% of the concomitant river discharge. The net spatially integrated material fluxes from the STE into the estuary were equivalent up to 45–110% of the concomitant riverine fluxes for DIC and TA, around 14–32% for DSi and 7–19% for DIN, and negligible for SRP. Paradoxically, the mixing lines along the salinity gradient revealed no apparent additions of these species. These additions are not revealed because the STE is a relatively small spatially-averaged source (at most 11% of the total input at steady state) that spreads throughout the estuary as a non-point source in contrast to the major point sources of the river and the ocean for the estuary and a true open ocean endmember is likely lacking. Greater water flushing in the summer might dilute the STE effect on the mixing lines even more. The great spatial variation in salinity in the estuary introduced the major uncertainty in our estimates of the flushing time, which further affected the estimate of the subterranean discharge and associated material fluxes. Additionally, the great spatial variation in the STE endmember caused the relatively large ranges in these flux estimates. Despite apparent conservative mixing of DIC, DIN, and DSi in estuaries, net subterranean exports must be taken into account in evaluating geochemical impacts of estuarine exports on shelf waters.

1. INTRODUCTION

Riverine fluxes into the coastal ocean through estuaries are a prime nutrient source for coastal ecosystems (Jickells, 1998). The estuarine export fluxes, however, may not be equivalent to the riverine fluxes because of some processes that remove nutrients and others that add them. An

Abbreviations: DIC, dissolved inorganic carbon; DIN, dissolved inorganic nitrogen; DSi, dissolved silicate; SRP, soluble reactive phosphorus; TA, total alkalinity; SGD, submarine groundwater discharge; TSM, total suspended matter; STE, subterranean estuary.

* Corresponding author at: College of Ocean and Earth Sciences, Xiamen University, Xiamen, China. Tel.: +86 592 2880160.
E-mail address: gzhwang@xmu.edu.cn (G. Wang).

http://dx.doi.org/10.1016/j.gca.2014.11.001
0016-7037/

often overlooked addition is from the subterranean estuary (STE), where mixing of freshwater and seawater is accompanied by biogeochemical processes. Microbial respiration in the STE increases concentrations of some elements at least an order of magnitude higher than their riverine counterparts, for example, DIC, TA, nutrients, and metals (Kelly and Moran, 2002; Moore, 2010; Liu et al., 2012; Sanders et al., 2012). The subterranean discharge, called submarine groundwater discharge (SGD), therefore, may carry significant amounts of materials into the surface estuary; indeed, it has been recognized as a significant material transport pathway for coastal waters (e.g., Burnett et al., 2003; Moore, 2010). SGD studies have been carried out in the Mississippi, Atchafalaya, Okatee, Chao Phraya, Wanquan, and many other estuaries (e.g. Krest et al., 1999; Dulaiova and Burnett, 2006; Moore et al., 2006; Su et al., 2011), but few studies have quantified the net exports of materials from the STE into the estuary. By net, we mean the difference between what is exported via SGD and what enters the STE from the overlying estuary. There has been no quantitative assessment of how net exports from the STE affect the estuary in terms of the element mixing along the salinity gradient.

We pose two research questions: (a) was there a seasonal pattern of net material exports from the STE? and (b) how would net subterranean exports of species affect their mixing in the estuary? To address these questions, we selected the Jiulong River estuary, with relatively small river discharge, to quantify net subterranean exports into the estuary. The reason for this selection is that estuaries with relatively small river discharge likely contain a full range of salinity within a geomorphologically constrained area so that effects of net exports from the STE on the estuary may be quantitatively assessed in terms of mixing along the salinity gradient. To estimate seasonal SGD fluxes, we conducted four cruises to investigate distributions of dissolved radium in the Jiulong River estuary. The effects of net STE exports on the estuary were evaluated in terms of DIC, TA, DIN (including nitrate, nitrite, and ammonia), SRP, and DSi in the summer and winter.

2. STUDY AREA

The Jiulong River flows over southeast China with two main tributaries, the North Stream and the West Stream, and discharges into the estuary. Flow continues through Xiamen Bay and further into the southern Taiwan Strait (Fig. 1). The watershed area is 1.47×10^{10} m^2 (Zhang, 1996). Average annual freshwater discharge is 1.47×10^{10} m^3, only about 1.6% of that of the Yangtze River (Zhang, 1996), but the areal DIN and SRP yield rates from the Jiulong River watershed are 3.1 and 6.1 times greater than those from the Yangtze River watershed (Yan et al., 2012). The greater areal nutrient yield rates are coincident with a higher population density in the watershed (Yan et al., 2012). As one of the major rivers flowing into the northern South China Sea, nutrient surveys have been conducted in the estuary since 1962 throughout the years (Yan et al., 2012, and references therein). However, there has been no assessment of the effect of net exports from the STE on the C, N, P, and Si budgets in the Jiulong River estuary.

The estuary is subtropical (annual temperature range of 13–32 °C) and macro-tidal (an average tidal range of 4.95 m) (Yang and Hu, 1996). The surface sediments are about 10 m thick, comprised mainly of sands, clayey silts, and silty clay (Cai et al., 1993). Most of the heavy minerals in the sediments are terrigenous, around half of which are silicates (Hong, 1993; Hong and Chen, 2003). These sediments overlie up to 30 m thick Holocene deposits on top of crystalline granite bedrock (Hong and Chen, 2003). There are no confined aquifers.

The meteoric groundwater flow from nearby Xiamen Island (area = 128 km^2, coastline length = 32 km) into

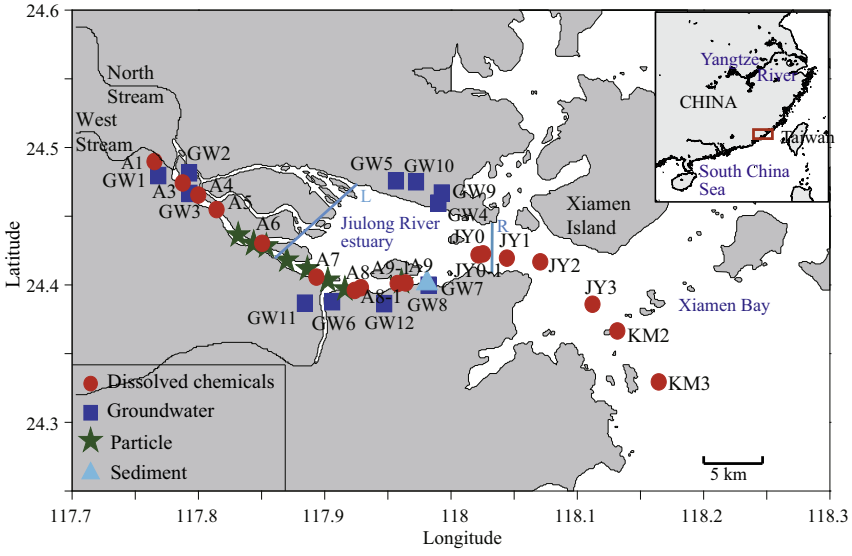

Fig. 1. Sampling stations in the Jiulong River estuary and the subterranean estuary. The main body of the estuary, the area between Transects L and R, is the domain of estuary for discussion.

Xiamen Bay was estimated to be 1.32×10^7 m^3 yr^{-1} based on a water balance model (Guo, 2002). SGD flux along the northern South China Sea coast (coastline length = 308 km) was quantified using both ^{226}Ra/^{228}Ra mass balance models and a three-end-member mixing model to be 2.2–3.7 $\times 10^8$ m^3 d^{-1}, 3–8% of which was fresh groundwater (Liu et al., 2012).

In this study stations were designed mainly in the water channel along the southern coast of the estuary, where the river and the ocean water interact most strongly. The northern estuary is very shallow and largely not navigable using our research vessel. We took the main body of the estuary between Transects L and R (surface area is 7.11×10^7 m^2) as the estuary domain for calculation and discussion (Fig. 1). Stations A7, A8, A8-1, A9, A9-1, JY0, and JY0-1 are located within the estuary domain. The average for these stations, if sampled, was taken to represent the estuary water. The average of samples, if collected, from stations JY1, JY2, JY3, KM2 and KM3, i.e., stations on the downstream (right) side of Transect R, was taken as the ocean end member. The average for stations A6, A5, A4, A3, and A1, i.e., stations on the upstream (left) side of Transect L, represented the river end-member. Station A1 on the west tributary was taken as the river mouth to serve as a reference point for distance.

3. MATERIALS AND METHODS

3.1. SGD tracer method

Natural radium isotopes serve well as tracers of subterranean discharge (Charette et al., 2008, and references therein). Radium is produced from the decay of thorium, a particle-reactive element. In most fresh water systems radium is particle-bound and its dissolved phase has relatively low activity. After particles encounter saline water through salt water intrusion into aquifers or particles moving from rivers to estuaries, radium desorbs and enters groundwater, estuarine and coastal waters in the dissolved phase. Radium is not chemically reactive in saline waters, so decreasing activities of dissolved radium offshore are due to mixing and decay (Moore, 1996; Krest et al., 1999). There are four radium isotopes, ^{223}Ra (half-life = 11.4 days), ^{224}Ra (half-life = 3.66 days), ^{226}Ra (half-life = 1600 yrs), and ^{228}Ra (half-life = 5.75 yrs).

3.2. Water column sample collection in the estuary and measurements

To investigate seasonal inventories of dissolved radium, samples were collected in July 2010, January 2011, April 2011, and November 2011 along the main channel in the Jiulong River estuary into Xiamen Bay (Fig. 1) on board R/V Ocean II. The weekly average river discharge just prior to each cruise was highest in July, 1048 m^3 s^{-1}, and lowest in January, 384 m^3 s^{-1} (Fig. 2). During each survey, the salinity gradient was well covered from the river mouth to Xiamen Bay (Fig. 3a), suggesting that the samples were representative of the entire estuary. Station A9-1 was sampled only in the summer and winter, JY0-1 only in the fall, and A8-1 only in the spring and winter. Station A4 was not sampled in the winter. Nutrients data collected in the first three cruises were analyzed and published in Yan et al. (2012).

Samples were collected and measured for dissolved radium isotopes, salinity, total suspended matter (TSM), DIC, TA, dissolved oxygen (DO) and particulate ^{224}Ra and ^{228}Th as described in detail in the Electronic Annex EA.1. To estimate changes of DIC due to photosynthesis/respiration, the apparent oxygen utilization (AOU) was calculated (see Eq. (EA.1.1)). If we assume that ^{224}Ra and ^{228}Th are at equilibrium on suspended particles in the river water, the fraction of desorbed ^{224}Ra in the estuary can be calculated (Eq. (EA.1.2)).

3.3. Sample collection in the STE and measurements

Samples were collected using a peristaltic pump at 12 domestic wells from surface aquifers around the Jiulong River estuary (Fig. 1) and measured for dissolved radium, DIC, TA, DIN, SRP, and DSi, with a few stations sampled at multiple times (Nov. 2011, March 2012, April 2012, and/

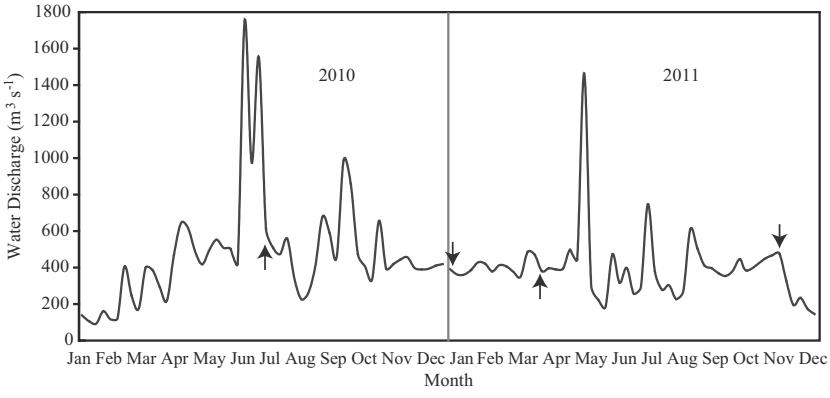

Fig. 2. The weekly average water discharge for the Jiulong River in 2010 and 2011. The average was calculated from discharge data provided at two downstream hydrological stations Punan and Zhengdian by the Bureau of Hydrology, Ministry of Water Resources, China at the website http://xxfb.hydroinfo.gov.cn. The arrows point to the cruise time when distributions of dissolved radium were investigated in the Jiulong River estuary.

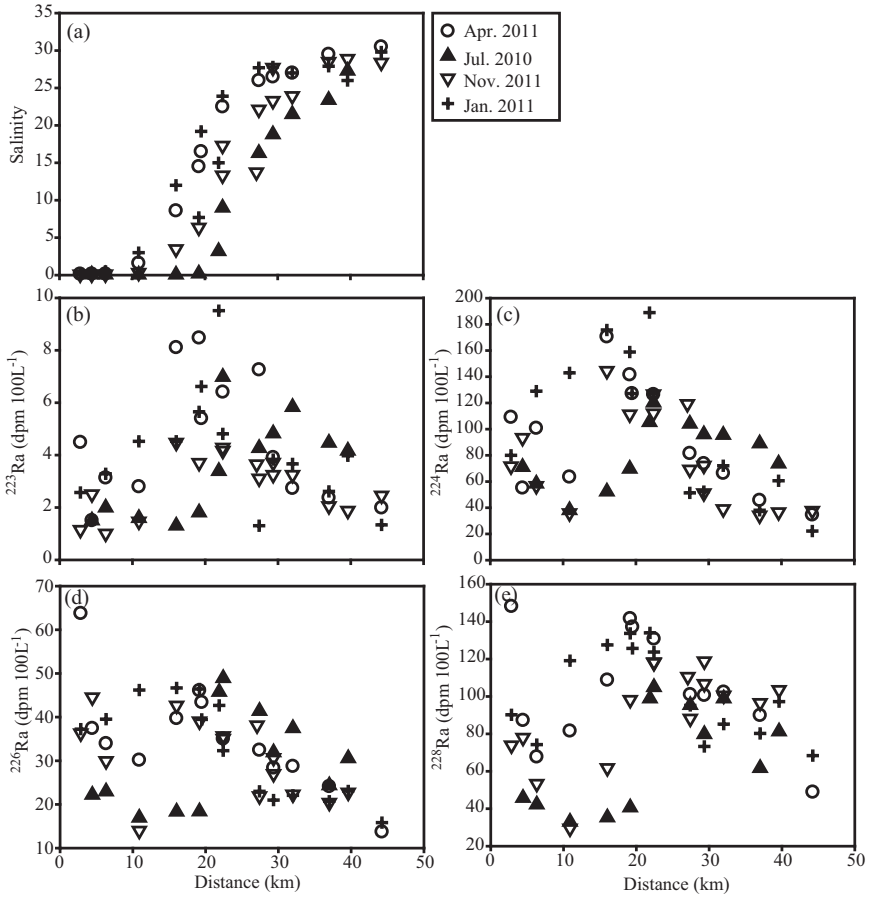

Fig. 3. Distributions of salinity and dissolved radium with the distance from the river mouth in the Jiulong River estuary in July 2010, January 2011, April 2011, and November 2011, (a) salinity, (b) ^{223}Ra, (c) ^{224}Ra, (d) ^{226}Ra, and (e) ^{228}Ra.

or July 2013) to evaluate seasonal variations of the chemical compositions (detailed sampling information is listed in Table 1). All the stations are within 2.5 km distance from the water channel with the potential to show mixing between meteoric groundwater and seawater. Three wells (GW1-3) are at least 7 km away from the estuary domain, used for comparison. The other wells, surrounding the estuary domain within a distance of 2.2 km, were taken to represent the STE affecting the estuary domain. At each station the well was purged for about 30 min before water samples were taken at about 1 m water depth. The samples were collected and measured in the same way as the estuary samples for dissolved radium, DIC, and TA with about 8 L water collected for radium. Nutrient samples were collected and measured as described in EA.1. To illustrate the intrusion of estuary water into the STE, an Aqua Troll 400 (In-Situ Inc.) was positioned at Station GW6 at a depth of 0.6 m below the water table to monitor changes of salinity and water level with the tidal height for 22 h.

3.4. SGD estimation using the mass balance of radium

In the estuary, the sources of dissolved radium might be diffusive inputs from sediments, desorption from suspended particles, and subterranean exports. The sink term for dissolved radium includes mixing with the ocean water and radioactive decay. Under the assumption of steady state, a mass-balance equation can be set up for the long-lived radium isotopes considering source and sink terms,

$$F_R \cdot {}^{i}\mathrm{Ra}_R + {}^{i}F_{\mathrm{sed}} \cdot A_E + F_R \cdot {}^{i}\mathrm{Ra}_d \cdot C_{\mathrm{TSM}} + F_{\mathrm{SGD}} \cdot {}^{i}\mathrm{Ra}_{\mathrm{STE}} = A_E \cdot H \cdot ({}^{i}\mathrm{Ra}_E - b \cdot {}^{i}\mathrm{Ra}_O) \cdot \frac{1}{T_f} \quad (1)$$

where F_R is the river water discharge, ${}^{i}Ra_R$ is the activity of dissolved ${}^{i}Ra$ of the river end-member, $i = 226$ and 228, ${}^{i}F_{sed}$ is the diffusive flux of ${}^{i}Ra$ from sediments, A_E is the sediment surface area of the estuary, 7.11×10^7 m^2, ${}^{i}Ra_d$ is the activity of desorbed ${}^{i}Ra$ from suspended particles, C_{TSM} is the concentration of TSM, F_{SGD} is the SGD flux, ${}^{i}Ra_{STE}$ is the activity of dissolved ${}^{i}Ra$ of the STE end-member, H is the water depth of the estuary, ${}^{i}Ra_E$ is the activity of dissolved ${}^{i}Ra$ of the estuary water, b is the return flow factor, ${}^{i}Ra_O$ is the activity of dissolved ${}^{i}Ra$ of the ocean end-member, T_f is the flushing time, and λ_i is the decay constant of ${}^{i}Ra$. The decay loss can be neglected for ^{226}Ra and ^{228}Ra due to their relatively long half-lives.

3.5. Flushing time estimation

Based on a tidal prism model, the flushing time can be estimated (Sanford et al., 1992) by

Table 1
Sampling stations and data collected in the STE.[a]

Station[b]	Latitude	Longitude	Distance	Depth	Time	S	^{223}Ra	^{224}Ra	^{226}Ra	^{228}Ra	DIC	TA	SRP	DSi	DIN
			km	m	yyyy-mm		dpm 100 L^{-1}				μM				
GW1	24.4796	117.7682	11.90	1.0	2012-03	0.1	3.1	53	18	41	5343	4128	34.7	709	903
					2012-04	0.2	2.0	125	19	52	6345	5645	35.7	798	578
					2013-07	0.2	0.4	48	17	51	6274	5573	41.5	879	581
					2011-10	0.2	1.3	85	23	65	6653	5613	33.3	827	nd
GW2	24.4816	117.7926	9.54	0.9	2012-03	0	2.4	20	18	23	4235	3876	0.2	337	111
					2013-07	0	1.6	17	10	11	3814	3213	5.2	630	396
GW3	24.4666	117.7929	7.72	1.0	2012-03	0.5	7.0	239	83	162	5350	4412	0.3	1028	111
					2011-10	0.5	5.8	147	73	172	5016	4207	0.7	936	nd
GW4	24.4595	117.9900	0.62	1.0	2012-03	0.2	4.6	225	65	146	3118	2600	75.4	631	1266
					2013-07	0.3	2.1	201	68	148	3872	2976	14.6	713	506
GW5	24.4758	117.9564	1.09	1.0	2012-03	0.1	2.3	77	64	61	2513	1808	26.1	370	1083
					2013-07	0.5	0.5	63	29	63	3170	nd	19.6	584	113
GW6-a	24.3852	117.9042	0.11	0.8	2012-04	6.5	95.3	1479	1829	2988	3319	2539	0.3	679	287
GW6-b	24.3878	117.9059	0.33	0.6	2012-04	8.2	178.8	2241	1808	2696	3344	2564	0.1	641	220
					2013-07	9.4	89.2	1176	1413	2502	5505	4783	0.0	539	274
GW7	24.3998	117.9822	0.16	1.0	2012-03	0.1	1.3	39	21	51	3224	2935	56.8	632	752
					2012-04	0.1	3.7	57	31	64	4395	2849	90.4	659	857
					2013-07	0.1	0.5	28	13	37	3170	2847	50.1	745	443
					2011-10	0.3	3.0	86	20	77	5918	5420	50.8	886	nd
GW8	24.3997	117.9823	0.20	1.0	2011-10	0	5.3	223	32	90	2701	1546	1.5	819	nd
GW9	24.4669	117.9927	1.33	1.0	2013-07	0.2	4.2	296	83	164	5970	5276	2.2	383	305
GW10	24.4751	117.9723	2.21	0.7	2013-07	0.5	3.1	73	28	68	4528	3801	5.7	455	510
GW11	24.3867	117.8843	1.53	1.0	2013-07	15.0	58.4	2106	870	2708	7882	7222	0.2	341	556
GW12	24.3864	117.9471	0.97	1.0	2013-07	0	4.0	152	83	155	2308	1501	0.5	724	44

[a] nd, not determined; "Distance" represents the distance to the estuary domain and "Depth" means the sampling depth.
[b] GW6-a and GW6-b are located in the same village, about 100 m away from each other.

$$T_f = \frac{A_E \cdot H \cdot T}{(1-b)\cdot V_P + F_R \cdot T} \quad (2)$$

where T is the tidal period, 12 h and 23 min, and V_P is the volume of the tidal prism. The mean tidal prism through Transect R calculated from a numerical model of Xiamen Bay (Jiang and Wai, 2005) is 3.33×10^8 m^3 using a tidal range of 3.9 m.

The return flow factor, b, is the fraction of the estuary water that returns to the estuary after export on the falling tide. To determine b, a three-end-member mixing model was set up, considering the mass balance of water, salt, and ^{228}Ra in the estuary with three end-members, the STE, the river, and the ocean,

$$\begin{cases} f_O + f_R + f_{STE} = 1 \\ S_O \cdot f_O + S_R \cdot f_R + S_{STE} \cdot f_{STE} = S_E \\ {}^{228}Ra_O \cdot f_O + {}^{228}Ra_R \cdot f_R + {}^{228}Ra_{STE} \cdot f_{STE} = {}^{228}Ra_E \end{cases} \quad (3)$$

where f is the fraction of each end-member in the estuary, S is salinity, ^{228}Ra is the activity of ^{228}Ra, the subscript '$_O$' means ocean endmember, '$_R$' – river endmember, '$_{STE}$' – STE endmember, and '$_E$' – estuary water. Similarly, the mass-balance of water, salt, and ^{226}Ra was set up to solve for fo, f_{STE}, and f_R. We assume that fo represents the fraction of water that returns to the estuary after export, i.e. $fo = b$ (Moore et al., 2006). After fo was determined in both ways, we substitute fo (=b) into Eq. (2) and solve for the flushing time. Desorption of ^{228}Ra and ^{226}Ra from particles had negligible effects on the flushing time (<0.1%) as justified using the winter data (see EA.2 for details), so desorption was not considered in the mass balance equations. Appendix Table A.1 lists values of the three endmembers and of the estuary water in each season. All the estuary data are provided in EA.3. Errors were derived using the method explained in EA.1.3.

4. RESULTS

4.1. Dissolved radium in the Jiulong River estuary

The seasonal sampling campaigns extended from the Jiulong River estuary into Xiamen Bay. The weekly average river water discharge just before each cruise was summer > fall > spring ≈ winter (Fig. 2). The seasonal sequence of salinity in the estuary is inverse to that of the river flow (Fig. 3a). In the summer the salinity increased with the distance from the river mouth from 0.07 in the upper estuary to 27.30 in Xiamen Bay. Due to lower river water discharges, the salinity in the estuary was slightly higher in other seasons than in the summer (Fig. 3a). Dissolved radium showed peaks in the mid estuary for the four isotopes (Fig. 3). In the upper estuary activities of dissolved radium were relatively low in the summer due to a greater river discharge of low radium waters and less desorption at near-zero salinities. In the lower estuary and Xiamen Bay, activities of dissolved radium decreased due to mixing with the ocean water that was relatively deplete in radium.

The bottom salinity at Station A9 was 17.3, higher than the surface salinity of 13.3. The activity of dissolved radium at the bottom depth was 112 dpm 100 L^{-1} for ^{224}Ra, 11% lower than the surface ^{224}Ra of 126 dpm 100 L^{-1}, while for the other radium isotopes the bottom values were almost the same as the surface values (Table EA.3.2). This indicates that although the estuary water was not vertically well mixed in terms of salinity, surface radium data represent the whole water column radium activity.

4.2. Desorbable radium from suspended particles in the Jiulong River estuary

The activity of particulate ^{228}Th was 5.32 dpm g^{-1} in the fresh water and decreased to 3.30 dpm g^{-1} at a salinity of 1.3. Further downstream the activity of particulate ^{228}Th decreased semi-exponentially with increasing salinity to 1.86 dpm g^{-1} at a salinity of 22.3 (Fig. EA.4). The decrease in the activity of particulate ^{228}Th with increasing salinity was likely caused by a decrease in the activity of its parent, particulate ^{228}Ra, with increasing salinity due to desorption into the dissolved phase. The activity of dissolved ^{228}Ra increased with salinity until reaching the mid-salinity zone (Fig. 3e). When the salinity further increased, the fraction that could be desorbed remained relatively constant. The activity of particulate ^{224}Ra followed a similar trend, decreasing from 4.21 dpm g^{-1} in the fresh water to 0.88 dpm g^{-1} at a salinity of 22.3 with the fraction of desorbed ^{224}Ra increasing from 0.2 to 0.5. The average salinities of the estuary water were greater than 2 in all four seasons, resulting in an average particulate ^{228}Th of 2.6 dpm g^{-1} and an average fraction of desorbed ^{224}Ra of 0.43. This fraction of desorbable Ra is comparable to the results of other investigations, e.g., 0.31–0.41 in Atchafalaya River and Yangtze River (Krest et al., 1999; Gu et al., 2012), likely due to similarity in sediment grains.

The fractions of desorbable ^{226}Ra and ^{228}Ra were assumed to be equal to those of ^{224}Ra. The maximum activities of particulate ^{226}Ra, 2.5 dpm g^{-1}, and ^{228}Ra, 2.09 dpm g^{-1}, in other rivers (Krest et al., 1999) were taken to be the activities in equilibrium with their parent nuclides and used here, so that $^{226}Ra_d = 2.5$ dpm $g^{-1} \times 0.43 = 1.1$ dpm g^{-1}, and $^{228}Ra_d = 2.09$ dpm $g^{-1} \times 0.43 = 0.90$ dpm g^{-1}.

4.3. Features of the STE

At Stations GW1–3, salinities ranged from 0 to 0.5, demonstrating slight seawater intrusion. Activities of dissolved radium varied by an order of magnitude (Table 1). At other GW stations around the estuary domain, the salinity ranged from 0 to 15.0. The radium activity varied by two orders of magnitude with much higher activities at salinity greater than 6. Other components behaved differently with respect to salinity. DIC, TA, and DSi varied greatly with salinity. SRP and DIN varied widely at low salinities and remained relatively low at high salinities (>6) (Table 1).

Based on the 22-h observation at GW6, the salinity and water level in the STE peaked in ebb tides with a minimum during flood tides (Fig. 4). The STE responded to surface

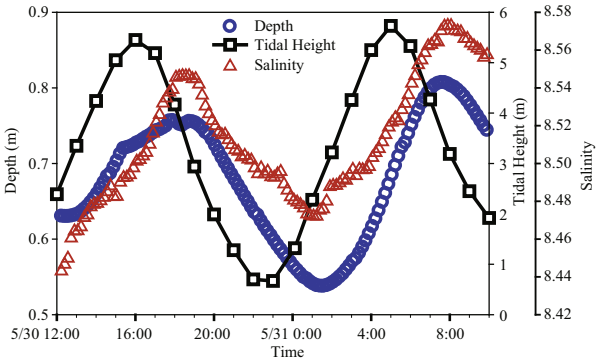

Fig. 4. Time series observations of salinity and water level in the subterranean estuary at Station GW6.

tides with a lag time of about 3 h. Seasonal variations were present in concentrations of chemical species at the STE stations (Table 1). However, even the greatest seasonal variation was not as great as the spatial variation. For example, the seasonal variation of dissolved radium fell within a factor of 2, while the spatial difference was at least an order of magnitude, when the salinity changed from 0 to 15.0. Because the spatial variation was much greater than the seasonal variation, the STE endmember was assumed to be constant with season.

The activities of ^{228}Ra vs. ^{226}Ra at all the GW stations, except GW11, were approximately linear with a regression slope of 1.6 (Fig. 5a), indicating similar compositions of the source aquifers. For the low salinity samples (with one sample collected at GW5 in March excluded as an outlier), with activities of ^{228}Ra and ^{226}Ra in the same order of magnitude as those of surface waters, the slope of ^{228}Ra vs. ^{226}Ra was 1.91, very close to that for surface waters of 1.89 (Fig. 5b). This similarity, as well as the overlapping of the ranges in the activities of ^{228}Ra and ^{226}Ra, respectively, of surface waters and of the low salinity groundwater, implied that radium in surface estuary waters were mainly sourced from the sampled STE waters. For a conservative estimate of SGD, we select the four saline groundwater samples as the STE endmember, taking the lowest salinity sample (S = 6.5, which was termed STE1) and the highest salinity sample (S = 15.0, which was termed STE2) as the range of the STE endmember. SGD was calculated considering the ranges in radium of the STE endmember and SGD-associated net material fluxes were calculated using the average concentration of these four saline samples (listed in Tables A.1 and A.2).

4.4. Flushing time of the Jiulong River estuary

For the flushing time estimates we need the return flow factor, b, which is derived from the fraction of ocean water that returns to the estuary on the rising tide. Calculations using STE1 gave the same fraction of the ocean water and the flushing time, within 1%, as those calculated using STE2 for each long-lived radium isotope. This indicates that the flushing time is not sensitive to the STE endmember. The fraction of the ocean water in the estuary calculated using

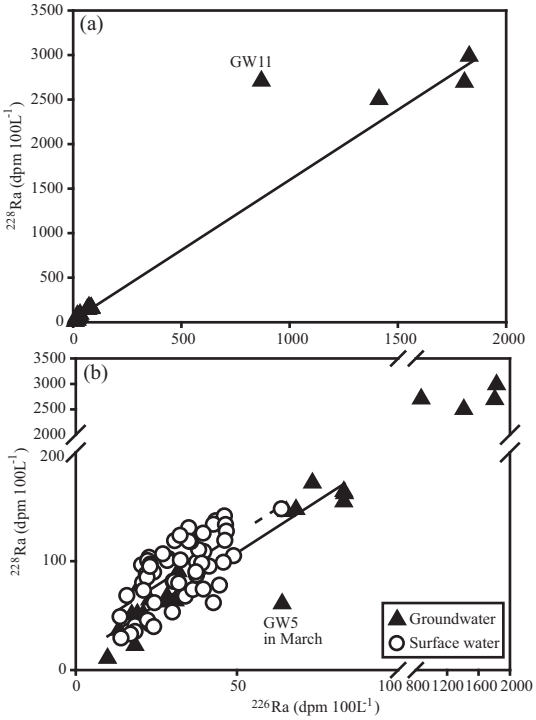

Fig. 5. Activities of ^{228}Ra vs. ^{226}Ra in the Jiulong River estuary and subterranean estuary, (a) data in the subterranean estuary, the solid line has a slope of 1.6 with GW11 excluded in the regression, and (b) data in the surface water compared with the data in the subterranean estuary, the solid line is the regression of data of the low-salinity (<1) groundwater with a slope of 1.91 and an r^2 of 0.94 with GW5 in March excluded in the regression, the dashed line is the regression of data of the surface water with a slope of 1.89 and an r^2 of 0.45.

^{226}Ra was almost the same as that based on ^{228}Ra using either STE endmember, 61% in the spring, 24–25% in the summer, 44% in the fall, and 61–62% in the winter (Fig. 6). The consistency indicates the reliability of our estimates. The error bars were calculated using the standard deviation of the spatial composition of the river, the ocean, and the estuary water listed in Table A.1. The fraction of the river endmember was summer > fall > winter > spring and greater than that of the ocean endmember in the summer and fall (Fig. 6) due to relatively high river water discharges. The fraction of the STE in the estuary was less than 0.01 in all four seasons.

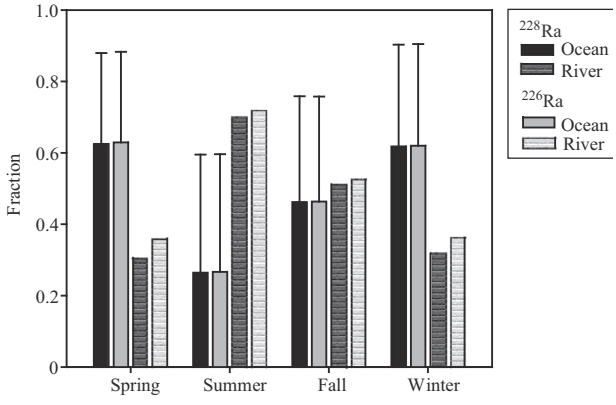

Fig. 6. Fractions of the ocean endmember and river endmember in the estuary estimated using ^{226}Ra and ^{228}Ra, respectively, in four seasons. The error bars were calculated from the standard deviation of the composition of the river, the ocean, and the estuary water.

The flushing time of the estuary calculated using the two radium isotopes was almost the same considering errors transferred from the fraction of the ocean water (Table 2), with the average of summer (0.78 ± 0.19 d) < fall (2.03 ± 0.63 d) < winter (2.05 ± 0.95 d) < spring (2.35 ± 0.94 d). The annual average water exchange time for the estuary has been estimated to be approximately 2 d based on a model considering the water and salt budgets of the estuary and a river water discharge of 1.44×10^{10} m^3 yr^{-1} (Cao et al., 2005); this falls within our calculated flushing time range.

4.5. Seasonal SGD flux

In solving SGD flux in Eq. (1), we assumed that there were no seasonal changes in ${}^{i}F_{sed}$, ${}^{i}Ra_{d}$, and ${}^{i}Ra_{STE}$. The diffusive fluxes from sediments of ^{226}Ra and ^{228}Ra used in the northern South China Sea in Liu et al. (2012) were adopted in this study, ${}^{226}F_{sed} = 0.45$ dpm m^{-2} d^{-1}, and ${}^{228}F_{sed} = 25$ dpm m^{-2} d^{-1}. TSM, H, ${}^{i}Ra_{R}$, ${}^{i}Ra_{O}$, and ${}^{i}Ra_{E}$ varied with season (Table A.1). So did T_f and F_R (Table 2). The SGD flux calculated is listed in Table 2. In general, the magnitude of the SGD flux into the Jiulong River estuary was on the order of 10^6–10^7 m^3 d^{-1}. A higher SGD flux usually followed a greater river discharge that may reflect episodic events such as heavy rains or storms (Fig. 7). This indicates that the SGD flux has a fast response to precipitation. Compared to the concomitant river discharge, the SGD flux estimated using ^{226}Ra, which is winter < spring < fall < summer, was equivalent to 8–19% of the river discharge (Table 2). The highest SGD in the summer and the lowest in the winter were also reported in the Okatee estuary, South Carolina, and the Pettaquamscutt estuary, Rhode Island, USA (Kelly and Moran, 2002; Moore et al., 2006). The maximum SGD in the summer may be driven by high sea level at these sites (Gonneea et al., 2013).

4.6. Seasonal distributions of DIC, TA, and DO in the estuary

At low salinities (<1) DIC ranged 479–641 μM in the summer and 1056–1392 μM in the winter, and TA scattered 401–539 μM in the summer and 917–1327 μM in the winter. Concentrations of both increased with salinity further downstream, almost falling on conservative mixing lines with minor additions (<100 μM) in the salinity range of 0–15 in the winter (Fig. 8a and b), with a greater intercept in the winter than in the summer.

Concentrations of DO scattered at low salinities (<1), 156–220 μM in the summer and 196–243 μM in the winter, and increased with salinity at higher salinities (>1) to 269 μM in the winter and remained low around 185 μM in the summer (Fig. 8c). AOU decreased in both seasons

Table 2
The flushing time (T_f) determined using ^{226}Ra and ^{228}Ra, respectively, and SGD fluxes into the Jiulong River estuary (F_{SGD}) estimated using radium box models considering the range of radium in the STE endmember, compared with river water discharges (F_R). The uncertainties in T_f were estimated considering the spatial variations in the composition of the river, the ocean, and the estuary water.

	^{226}Ra-F_{SGD}	^{228}Ra-F_{SGD}	F_R	^{226}Ra-T_f	^{228}Ra-T_f
	10^7 m^3 d^{-1}			d	
Spring	0.29–0.60	0.57–0.67	3.36	2.34 ± 1.31–2.37 ± 1.34	2.33 ± 1.30–2.36 ± 1.33
Summer	0.69–1.44	0.92–1.09	9.05	0.77 ± 0.27–0.78 ± 0.27	0.77 ± 0.27–0.78 ± 0.27
Fall	0.45–0.93	0.59–0.69	4.97	2.02 ± 0.88–2.03 ± 0.89	2.03 ± 0.89
Winter	0.26–0.54	0.56–0.66	3.32	2.04 ± 1.32–2.06 ± 1.35	2.03 ± 1.31–2.05 ± 1.34

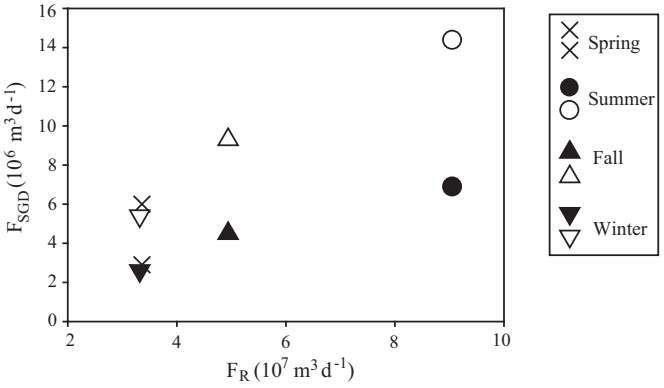

Fig. 7. The relation between the river discharge (F_R) and the flux of SGD (F_{SGD}), with ^{226}Ra-F_{SGD} as an example. The range of F_{SGD} in each season is calculated considering the range in the STE endmember.

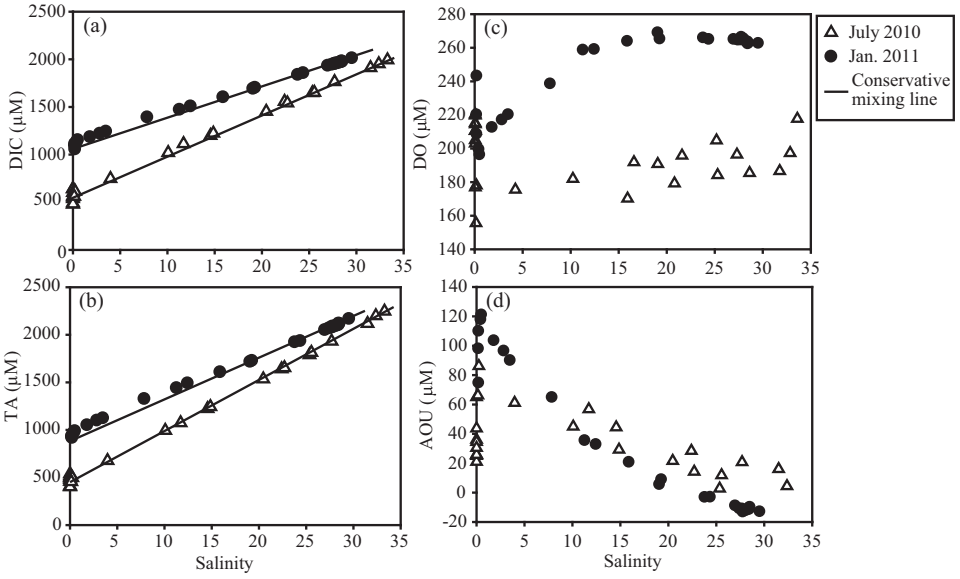

Fig. 8. Distributions of DIC, TA, DO and AOU vs. salinity in the Jiulong River estuary in July 2010 and January 2011, (a) DIC, (b) TA, (c) DO, and (d) AOU.

with increasing salinity, i.e., further away from the river mouth (Fig. 8d), similar to what was present in the Pearl River estuary (Chen et al., 2008). AOU was positive in the summer, decreasing from 86 to 3 μM with increasing salinity, indicating respiration dominance in the estuary; this relative dominance decreased from the river mouth toward the ocean. The concentration of Chl. *a* followed the same pattern, decreasing from 11.49 to 2.13 μg L^{-1} (Mo et al., 2013). In the winter a negative AOU at salinities of >23 indicated the relative dominance of photosynthesis; however the maximum was only 13 μM, implying that the primary production was low. An even lower Chl. *a*

reinforced this conclusion (Huang B., unpublished data). This low biological activity is consistent with conservative mixing behaviors of DIN and DSi in the estuary presented in Yan et al. (2012).

5. DISCUSSION

5.1. Net export fluxes of DIC, TA, DIN, SRP, and DSi from the STE into the Jiulong River estuary

SGD includes two components, meteoric groundwater and sea water that has infiltrated the aquifer. These components mix in the STE and react with the aquifer solids to produce salty SGD. The rhythmic coincidence of salinity and water level in the STE station GW6 (Fig. 4) revealed the movement of the saltwater interface in the aquifer. Unless there is a freshwater spring or seep, neither of which was observed in this area, subterranean discharge will be brackish to salty. Here we assume that all of the SGD passes through the STE and neglect any seepage of freshwater directly into the ocean. By using radium as a tracer, we focus on this brackish to saline groundwater discharge. By neglecting fresh groundwater discharge and using the brackish groundwater as endmembers, we produce a minimum estimate of the total SGD.

To assess the minimum effects of net material export fluxes from the STE on the estuary, the minimum SGD values, estimated using ^{226}Ra, were utilized in later calculations. The minimum SGD was 0.69–1.44 $\times 10^7$ m^3 d^{-1} in the summer and 0.26–0.54 $\times 10^7$ m^3 d^{-1} in the winter. Dividing by the surface area of the estuary domain produces an advective velocity of 0.04–0.08 m d^{-1} in the winter and about twice that in the summer, 0.10–0.20 m d^{-1}. The fraction of fresh groundwater in the SGD ranged from 0–47% in the summer to 0–54% in the winter as estimated from salinity. The higher SGD discharge rate coincided with a higher degree of estuary water intrusion into the aquifer, illustrated by a smaller fraction of fresh groundwater in the STE. This coincidence resembled the model result of SGD driven by sea level in an unconfined coastal aquifer at Waquoit Bay, US, by Gonneea et al. (2013).

The net subterranean export material flux estimates were derived from the difference between SGD associated material fluxes and the return fluxes from the estuary to the STE. The SGD associated material fluxes were calculated by the SGD flux multiplied by the concentration of chemical species in the STE. The flux from the estuary to the STE was calculated by the SGD flux multiplied by the fraction of the estuary saline water in the STE and the estuarine bottom concentration. Note that using "estuarine bottom concentration" for the estuarine endmember may neglect DIC produced at the sediment–water interface that is subsequently transported into the STE. For DIC the SGD-associated flux was 1.32–2.72 $\times 10^7$ mol d^{-1} in the winter, when the average bottom concentration was 1759 μM. Thus, the net export DIC flux from the STE was calculated to be 0.86–2.28 $\times 10^7$ mol d^{-1} (0.12–0.32 mol m^{-2} d^{-1}), or 65–84% of the total SGD-associated DIC flux. Similarly, the net DIC exported from the STE in the summer was 78–88% of the total DIC flux carried by SGD (Table 3). The net subterranean export flux of TA was 58–81% in the winter and 74–86% in the summer of the total SGD-associated TA flux. The riverine material fluxes calculated by the concentration at the station closest to the river mouth multiplied by the river water discharge are shown in Table 3. In the summer, the net STE export fluxes of DIC and TA were equivalent to 45–110% of the concomitant riverine fluxes. In the winter, the riverine fluxes of DIC and TA were about twice to five times as high as the net exports from the STE.

The net export flux of SRP from the STE was negative in both seasons on the order of -10^3 mol d^{-1}, indicating that the flux was from the estuary to the STE. Pronounced additions of SRP occurred in the estuary in both seasons (Yan et al., 2012). However, this addition of SRP could not result from SGD based on this study. Particle sorption/desorption, as suggested by Yan et al. (2012), might be a likely source. The net DSi and DIN fluxes exported from the STE were on the order of 10^6 mol d^{-1}, around one tenth to one third of the concomitant riverine fluxes for DSi and less than 20% of the riverine fluxes for DIN (Table 3). However, because denitrification might occur in the STE with N_2 produced (Porubsky et al., 2011), a factor not measured in this study, the actual export DIN fluxes could be

Table 3
SGD-associated material fluxes (F_{mSGD}) and net material fluxes exported from the STE into the Jiulong River estuary (NF_{mSTE}), riverine fluxes (F_{mR}), estimated input rate (IR) from the STE to the estuary, and replacement rate of chemical species (RR) in the estuary in the summer and winter.

		DIC	TA	SRP	DSi	DIN
Summer	F_{mSGD} (mol d^{-1})	3.46–7.23 $\times 10^7$	2.95–6.17 $\times 10^7$	1.16–2.43 $\times 10^3$	3.79–7.93 $\times 10^6$	2.31–4.82 $\times 10^6$
	NF_{mSTE} (mol d^{-1})	2.69–6.38 $\times 10^7$	2.19–5.32 $\times 10^7$	−8.77 to −8.63 $\times 10^3$	3.02–7.06 $\times 10^6$	1.47–3.89 $\times 10^6$
	F_{mR} (mol d^{-1})[a]	5.8 $\times 10^7$	4.9 $\times 10^7$	1.6 $\times 10^5$	2.2 $\times 10^7$	2.0 $\times 10^7$
	IR (μM d^{-1})	60.1–142.4	48.9–119	−1.92 to −1.93 $\times 10^{-2}$	6.7–15.8	3.3–8.7
	RR (μM d^{-1})	1219	1182	1.59	229	165
Winter	F_{mSGD} (mol d^{-1})	1.32–2.72 $\times 10^7$	1.13–2.32 $\times 10^7$	4.46–9.15 $\times 10^2$	1.45–2.98 $\times 10^6$	0.88–1.81 $\times 10^6$
	NF_{mSTE} (mol d^{-1})	0.86–2.28 $\times 10^7$	0.65–1.87 $\times 10^7$	−3.36 to −2.66 $\times 10^3$	1.15–2.70 $\times 10^6$	0.56–1.51 $\times 10^6$
	F_{mR} (mol d^{-1})[a]	3.5 $\times 10^7$	3.0 $\times 10^7$	5.4 $\times 10^4$	1.0 $\times 10^7$	1.1 $\times 10^7$
	IR (μM d^{-1})	14.9–39.5	11.3–32.3	−5.80 to −4.60 $\times 10^{-3}$	2.0–4.7	1.0–2.6
	RR (μM d^{-1})	852	878	0.74	71	62

[a] Data for SRP, DSi, and DIN are from Yan et al. (2012).

smaller than we report. In general, the net export material fluxes from the STE were higher in the summer than in the winter, almost equivalent to the riverine fluxes for DIC and TA and about one quarter of the riverine fluxes for DSi and DIN.

5.2. Paradox between the net subterranean exports and conservative mixing behaviors in the Jiulong River estuary

Considering the considerable fluxes from the STE into the estuary, one might expect to see signals of apparent addition relative to assumed conservative mixing lines along the salinity gradient in the estuary. However, in distributions of DIC and TA vs. salinity in the estuary (Fig. 8), only minor additions (<100 μM) appeared for DIC and TA in the low salinity range of 0–15 in the winter and there seemed to be conservative mixing in the summer. DSi and DIN appeared to be conservatively mixed in the estuary, although they varied greatly around salinity of 0 with differences in concentration of up to 50 μM for DSi and 100 μM for DIN (Yan et al., 2012). To address this paradox, we tried a simple calculation. The net DIC flux from the STE was divided by the volume of the estuary to get a net spatially-averaged DIC input rate from the STE of 14.9–39.5 μM d^{-1} in the winter and 60.1–142.4 μM d^{-1} in the summer. Using the average DIC concentration in the estuary divided by the flushing time, a replacement rate of DIC in the estuary was calculated to be 852 μM d^{-1} in the winter and 1219 μM d^{-1} in the summer. Under the assumption of steady state, the net input from the STE accounted for at most 5% in the winter to 11% in the summer of the total DIC input in the estuary. Moreover, SGD was a non-point source in the estuary because of the unconfined aquifer, which implied that unlike the river, the net DIC and salinity addition from the STE occurred throughout the estuary. With a relatively small spatially-averaged STE flux, the relation between DIC and salinity in the estuary would be approximately linear as derived from a one-dimensional diffusion model under the assumption of steady state (see EA.1.4). Furthermore, a true open ocean endmember is likely lacking as may be inferred from the relatively low salinity of the ocean endmember so that the addition that occurred throughout the estuary was not apparent on the overestimated mixing line. Therefore, there would be no apparent signals of major addition relative to the mixing curve for the salinity range in the estuary. Besides the above reasons, there might be one or more of the following reasons for this paradox: (a) the DIC river endmember was overestimated; (b) the CO_2 efflux, as one likely sink of DIC in the estuary, would balance some subterranean export. The minor addition in the winter may be caused by less river flushing. Similar calculations for TA, DSi, and DIN (Table 3) show that in general their net exports from the STE accounted for at most 10% of the total input rates in the estuary. All the calculations and discussion are based on the assumption of steady state. If the system is not at steady state, however, there may be no paradox.

TA and DIC in the STE correlated very well with a regression slope of 0.98 and an r^2 of 0.96, indicating that DIC and TA were produced in about 1:1 ratio in the STE regardless of season. In the estuary, a good linear correlation was also present for TA and DIC in both summer and winter seasons with an r^2 of at least 0.998. However, the regression slope varied from 1.34 in the winter to 1.22 in the summer. This difference in the relation of TA and DIC in the STE and the estuary confirmed that exports from the STE, as a non-point source to the estuary, did not play a dominant role in regulating the distribution of inorganic carbon in the estuary.

If extrapolated to even higher salinity, DIC and TA seemed to have a stable ocean end-member throughout the year. The ocean end-member also appeared to have stable concentrations of DSi, DIN, and SRP (Yan et al., 2012). The presence of the stable ocean end-member was caused by relatively small seasonal variations of the constituents of the ocean water. The ocean water with relatively constant composition and the river water with seasonally varying constituents served as point sources for the estuary, while exports from unconfined aquifers were non-point sources for the estuary, therefore did not show up as apparent additions on the mixing lines. Nevertheless, the large net exports from the subterranean estuary, which are up to 45–110% of the riverine fluxes of DIC and TA, and about 19–30% of the riverine fluxes of DIN and DSi, cannot be overlooked when evaluating geochemical impacts of estuarine exports on shelf waters.

5.3. Uncertainty analysis

From Eq. (1), the uncertainty in the SGD flux can result from the uncertainty in every other parameter in the

Table A.1
Salinities and activities[a] of ^{226}Ra and ^{228}Ra of the estuary water and of the river, ocean, and STE endmembers, TSM[b] of the river endmember and H[c] of the estuary domain used in the three-endmember mixing models and/or radium box models.

Season	River			
	S	^{226}Ra	^{228}Ra	TSM
Spring	0.51 ± 0.73	41.3 ± 15.2	96.2 ± 35.6	119.1
Summer	0.07 ± 0.003	21.6 ± 3.2	40.2 ± 5.4	104.5
Fall	0.15 ± 0.11	31.2 ± 12.9	58.7 ± 22.3	131.8
Winter	1.23 ± 1.54	41.0 ± 4.7	94.5 ± 22.7	322.5
	Estuary			H
Spring	17.62 ± 6.83	39.3 ± 5.7	123.9 ± 17.9	9.43
Summer	5.75 ± 6.92	34.6 ± 15.0	75.1 ± 34.1	6.30
Fall	11.80 ± 7.27	35.3 ± 8.0	95.4 ± 22.1	11.77
Winter	17.58 ± 7.49	38.4 ± 9.2	123.3 ± 14.4	8.13
	Ocean			
Spring	28.38 ± 1.93	23.7 ± 7.0	85.5 ± 25.0	NA[d]
Summer	22.75 ± 3.57	31.1 ± 5.4	80.5 ± 15.2	
Fall	26.59 ± 2.75	23.1 ± 2.8	101.8 ± 4.3	
Winter	27.70 ± 1.40	20.5 ± 2.8	80.9 ± 11.2	
	STE[e]			
	6.5–15.0	870–1829	2502–2988	
Average	9.80 ± 3.73	1480 ± 450	2724 ± 200	NA[d]

[a] Unit in dpm $100\ L^{-1}$.
[b] Unit in mg L^{-1}.
[c] Unit in m.
[d] NA: not applicable.
[e] The range is from the four saline STE samples.

Table A.2
Concentrations[a] of chemical species and salinity in the STE and in the bottom water of the estuary.

		DIC	TA	DIN	DSi	SRP	S
STE		5013 ± 2170	4277 ± 2228	334 ± 151	550 ± 151	0.17 ± 0.14	9.80 ± 3.73
Estuary	Summer	1108 ± 135	1098 ± 135	112 ± 36	152 ± 69	1.21 ± 0.20	12.20 ± 6.92
	Winter	1759 ± 199	1813 ± 262	122 ± 68	112 ± 62	1.44 ± 0.22	14.25 ± 7.49

[a] Unit in μM.

equation. Here the uncertainty in F_R, A_E, H, λ_i and C_{TSM} are taken as 0. The uncertainties in ${}^{i}Ra_R$, ${}^{i}Ra_E$, and ${}^{i}Ra_O$ are listed in Table A.1. Using the error propagation, Eq. (EA.1.3), the uncertainty in b was estimated to be 40–64% except in the summer when the uncertainty was up to 125%, and the uncertainty in T_f was 35–65% (Table 2). The major uncertainty in b and T_f is from the spatial variation of the salinity in the estuary (Table EA.1.1). Diffusion from sediments accounts for less than 10% of the source flux of radium; consequently, its contribution to the uncertainty in SGD is minor and was not evaluated. The uncertainty in the STE endmember is the largest source of uncertainty in SGD studies on continental shelves (e.g., Gu et al., 2012; Liu et al., 2012). In our study, the largest uncertainty in SGD is from the spatial variation of salinity in the estuary, followed by the uncertainty from the radium in the estuary and STE (Table EA.1.1).

The uncertainty in the net subterranean export material fluxes results not only from the parameters involved in Eq. (1), but also from the concentration of these materials in the STE and in the bottom water of the estuary, as well as from the salinity of the bottom water of the estuary. The major uncertainty is still from the spatial variation of salinity in the estuary, followed by the uncertainty from the concentration of these materials in the STE and from radium in the estuary and STE (Table EA.1.1). These uncertainties, however, would not change the conclusions reached based on the material fluxes calculated using the average chemical concentrations.

ACKNOWLEDGEMENTS

We thank the crew on R/V Ocean II for their assistance in the cruises. Discussions with Nengwang Chen, Minhan Dai, Shuh-Ji Kao, Peng Cheng, and Chen-Tung Arthur Chen helped to refine the manuscript. We are thankful to the associate editors, Jan G. Wiederhold and Peter Hernes, and four anonymous reviewers for their constructive suggestions and comments that greatly improve the manuscript. Shuling Wang helped in sample collection and measurements. This study was supported by the National Basic Research Program of China (2009CB421204) and the National Natural Science Foundation of China (41006041 and 40810069004). The sampling was partially supported by the Science Fund for Creative Research Groups of the National Natural Science Foundation of China (41121091) and the Fundamental Research Funds for the Central Universities of China (2012121054). The July 2010 cruise was supported by the National Natural Science Foundation of China (40949901).

APPENDIX A.

See Tables A.1 and A.2.

APPENDIX B. SUPPLEMENTARY DATA

Supplementary data associated with this article can be found, in the online version, at http://dx.doi.org/10.1016/j.gca.2014.11.001.

REFERENCES

Burnett W. C., Bokuniewicz H., Huettel M., Moore W. S. and Taniguchi M. (2003) Groundwater and pore water inputs to the coastal zone. *Biogeochemistry* **66**, 3–33.

Cai A., Zhang J., Shi Q., Zhu K. and Wang K. (1993) Research on the sedimentary and acoustic characteristics of new deposit sequence in Jiulongjiang Estuary and Xiamen Bay. *J. Xiamen U.* **32**(3), 345–350 (in Chinese with English abstract).

Cao W., Hong H. and Yue S. (2005) Modeling agricultural nitrogen contributions to the Jiulong River estuary and coastal water. *Glob. Planet. Change* **47**, 111–121.

Charette M. A., Moore W. S. and Burnett W. C. (2008) Uranium- and thorium-series nuclides as tracers of submarine groundwater discharge. In *U–Th Series Nuclides in Aquatic Systems* (eds. S. Krishnaswami and J. K. Cochran). Elsevier, Amsterdam, pp. 155–192.

Chen C.-T. A., Wang S.-L., Lu X.-X., Zhang S.-R., Liu H.-K., Tseng H.-C., Wang B.-J. and Huang H.-I. (2008) Hydrogeochemistry and greenhouse gases of the Pearl River, its estuary and beyond. *Quaternary International* **186**, 79–90.

Dulaiova H. and Burnett W. C. (2006) Radon loss across the water-air interface (Gulf of Thailand) estimated experimentally from ^{222}Rn–^{224}Ra. *Geophys. Res. Lett.* **33**, L05606. http://dx.doi.org/10.1029/2005GL025023.

Gonneea M. E., Mulligan A. E. and Charette M. A. (2013) Climate-driven sea level anomalies modulate coastal groundwater dynamics and discharge. *Geophys. Res. Lett.* **40**, 2701–2706. http://dx.doi.org/10.1002/grl.50192.

Gu H., Moore W. S., Zhang L., Du J. and Zhang J. (2012) Using radium isotopes to estimate the residence time and the contribution of SGD in the Changjiang effluent plume to the East China Sea. *Cont. Shelf Res.* **235**, 95–107.

Guo Z. (2002) Study on interactions between groundwater and seawater. Postdoc dissertation. Xiamen University, 1-41 (in Chinese).

Hong H. (1993) Study on heavy minerals in Xiamen Harbor. *Chin. Acta Oceanol. Sin.* **15**(3), 49–62 (in Chinese).

Hong H. and Chen F. (2003) Characteristics of heavy minerals in a core from Jiulongjiang Estuary. *Chin. J. Oceanogr. Taiwan Strait* **22**(1), 65–78 (in Chinese).

Jiang Y. and Wai W. (2005) Drying–wetting approach for 3D finite element sigma coordinate model for estuaries with large tidal flats. *Adv. Water Resour.* **28**, 779–792.

Jickells T. D. (1998) Nutrient biogeochemistry of the coastal zone. *Science* **281**, 217–222.

Kelly R. P. and Moran S. B. (2002) Seasonal changes in groundwater input to a well-mixed estuary estimated using radium isotopes and implications for coastal nutrient budgets. *Limnol. Oceanogr.* **47**, 1796–1807.

Krest J. M., Moore W. S. and Rama (1999) ^{226}Ra and ^{228}Ra in the mixing zones of the Mississippi and Atchafalaya Rivers: indicators of groundwater input. *Mar. Chem.* **64**, 129–152.

Liu Q., Dai M., Chen W., Huh C.-A., Wang G., Li Q. and Charette M. A. (2012) How significant is submarine groundwater discharge and its associated dissolved inorganic carbon in a river-dominated shelf system? *Biogeosciences* **9**, 1777–1795. http://dx.doi.org/10.5194/bg-9-1777-2012.

Mo Y., Lin L., Zheng L. and Huang B. (2013) Phytoplankton phosphorus stress of Jiulongjiang river-estuary and adjacent waters system in summer. *Oceanol. Limnol. Sin.* **44**, 214–248 (in Chinese).

Moore W. S. (1996) Large groundwater inputs to coastal waters revealed by ^{226}Ra enrichments. *Nature* **380**, 612–614.

Moore W. S. (2010) The effect of submarine groundwater discharge on the ocean. *Annu. Rev. Mar. Sci.* **2**, 345–374.

Moore W. S., Blanton J. O. and Joye S. B. (2006) Estimates of flushing times, submarine groundwater discharge, and nutrient fluxes to Okatee Estuary, South Carolina. *J. Geophys. Res.* **111**, C09006. http://dx.doi.org/10.1029/2005JC003041.

Porubsky W. P., Joye S. B., Moore W. S., Tuncay K. and Meile C. (2011) Field measurements and modeling of groundwater flow and biogeochemistry at Moses Hammock, a backbarrier island on the Georgia coast. *Biogeochemistry* **104**, 69–90.

Sanders C. J., Santos I. R., Barcellos R. and Filho E. V. S. (2012) Elevated concentrations of dissolved Ba, Fe and Mn in a mangrove subterrrenean estuary: Consequence of sea level rise? *Cont. Shelf Res.* **43**, 86–94.

Sanford L., Boicourt W. and Rives S. (1992) Model for estimating tidal flushing of small embayments. *J. Waterw. Port Coastal Ocean Eng.* **118**, 635–654.

Su N., Du J., Moore W. S., Liu S. and Zhang J. (2011) An examination of groundwater discharge and the associated nutrient fluxes into the estuaries of eastern Hainan Island, China using 226Ra. *Sci. Total Environ.* http://dx.doi.org/10.1016/j.scitotenv.2011.06.017.

Yan X., Zhai W., Hong H., Li Y., Guo W. and Huang X. (2012) Distribution, fluxes and decadal changes of nutrients in the Jiulong River Estuary, Southwest Taiwan Strait. *Chin. Sci. Bull.* **57**, 2307–2318. http://dx.doi.org/10.1007/s11434-012-5084-4.

Yang Y. and Hu M. (1996) Biogeochemical research in the Jiulong River estuary. In *Biogeochemical Research in Main Estuaries in China* (ed. J. Zhang). Chinese Ocean Press, Beijing, pp. 54–78.

Zhang J. (1996) Nutrient elements in large Chinese estuaries. *Cont. Shelf Res.* **16**, 1023–1045.

Associate editors: Jan G. Wiederhold & Peter Hernes